

Extraction and analysis of tree canopy height information in high-voltage transmission-line corridors by using integrated optical remote sensing and LiDAR

Jinpeng Hao^a, Xiuguang Li^a, Hong Wu^a, Kai Yang^a, Yumeng Zeng^b, Yu Wang^b, Yuanjin Pan^{c, d, *}

^a State Grid Ningxia Electric Power Research Institute, Yinchuan 750011, China

^b School of Electrical Engineering and Automation, Wuhan University, Wuhan 430061, China

^c School of Geodesy and Geomatics, Wuhan University, Wuhan 430079, China

^d Hubei Luofia Laboratory, Wuhan University, Wuhan 430079, China



ARTICLE INFO

Article history:

Received 21 October 2022

Accepted 24 November 2022

Available online 3 January 2023

Keywords:
UAV
LiDAR
Power line
Tree height

ABSTRACT

Traditional inspection methods cannot quickly and accurately monitor tree barriers and safeguard the transmission lines. To solve these problems, in this study, we proposed a rapid canopy height information extraction method using optical remote sensing and LiDAR, and used UAV optical imagery with LiDAR to monitor the height of trees in a university and a high-voltage transmission line corridor in the Ningxia region. The results showed that the relative error of tree height extraction using UAV optical images was less than 5%, and the lowest relative error was 0.11%. The determination coefficient R^2 between the optical image tree height extraction results and the measured tree height was 0.97, thus indicating a high correlation for both. In the field of tree barrier monitoring, the determination coefficient R^2 of tree height extracted using airborne LiDAR point cloud, and canopy height model (CHM) and of the measured tree height were 0.947 and 0.931, respectively. The maximum and minimum relative error in tree height extraction performed using point cloud was 2.91% and 0.2%, respectively, with an extraction accuracy of over 95%. The experimental results demonstrated that it is feasible to use UAV optical remote sensing and LiDAR in monitoring tree barriers and tree height information extraction quickly and accurately, which is of great significance for the risk assessment and early warning of tree barriers in transmission-line corridors.

© 2022 Editorial office of Geodesy and Geodynamics. Publishing services by Elsevier B.V. on behalf of KeAi Communications Co. Ltd. This is an open access article under the CC BY-NC-ND license (<http://creativecommons.org/licenses/by-nc-nd/4.0/>).

1. Introduction

With the rapid development of China's economy, energy demand is increasing continuously. The network of ultra-high voltage (UHV) high-capacity transmission lines has significantly expanded to ensure an uninterrupted energy supply in recent years [1,2]. The

rapid advances in power transmission technology have made inspection and maintenance of transmission lines challenging. Tree barriers constitute one of the main challenges for high-voltage transmission lines operating in mountainous areas with dense vegetation. When vegetation around power lines grows to a certain height, it may cause short circuits in transmission lines and even cause tree discharge, forest fire, and other problems [3,4], thus posing a threat to the ecosystem and property [5,6]. Tree barriers have caused considerable losses to the power department. Therefore, how to predict the risk posed by tree barriers is of immense research value in the power sector [7,8].

Tall trees threaten the transmission grid's safe operation, causing trips, discharges, and other accidents. Accidents caused by transmission line failures have been reported in many countries. For example, short circuits in power lines caused at least three historic fires in California, USA, affected the lives of tens of millions of people and generated substantial economic losses and

* Corresponding author. School of Geodesy and Geomatics, Wuhan University, Wuhan, 430079, China.

E-mail address: yjpan@whu.edu.cn (Y. Pan).

Peer review under responsibility of Institute of Seismology, China Earthquake Administration.



Production and Hosting by Elsevier on behalf of KeAi

irreversible damage to the environment [9,10]. In recent years, transmission line accidents caused by tree barriers have become increasingly frequent in China, posing a considerable challenge in ensuring safe power transmission. In March 2020, a forest fire in Xichang, Liangshan Prefecture, caused by a power failure, killed 19 people and caused economic losses of more than 90 million yuan. Thus, quick and accurate estimation of the height of trees in transmission corridors and timely clearing of tree barriers to reduce transmission line failures and enhance transmission security is of great significance for ensuring uninterrupted and safe power supply [11,12].

For monitoring and early warning against the risk posed by tree barriers, the height of trees over a large area must be obtained quickly and accurately. Methods for measuring the height of trees mainly include traditional measurements and remote sensing inversions. Traditional canopy height measurement relies on the manual use of optical measuring instruments (e.g., altimeters or laser range finders) to calculate the height of trees. As such, traditional canopy height measurement is labor- and resource-intensive and inefficient; moreover, the measurement accuracy is affected by the quality of the instruments and human factors [13–15]. Airborne laser radar and ground-based radar can be used to quickly obtain dense point clouds with three-dimensional (3D) coordinates for accurate tree height extraction; however, they are costly and require multiple rounds of acquisition to determine large-scale features, which is costly in the case of airborne Light Detection And Ranging (LiDAR) [16–18]. Existing remote sensing inversion techniques, such as polarimetric interferometric synthetic aperture radar, can retrieve canopy height information over large areas; however, most of them are still in the experimental stage and do not yield sufficiently high accuracy in practical applications [19–21].

In recent years, Unmanned Aerial Vehicle (UAV) technology has been continuously improved. Compared with traditional measurement methods, UAV remote sensing offers the advantages of low cost, high resolution, convenient operation, and flexible acquisition cycle; moreover, it is more efficient and has been widely employed in topographic mapping, agricultural production, and other fields [22–25]. Zhao et al. obtained the tree height data using UAV imagery and compared the results with the actual tree height measurement data obtained from the total station; experimental results revealed that consumer drones could be used for tree height monitoring with high accuracy [26]. Xie et al. used UAV remote sensing to obtain images of the study area, established the digital surface model (DSM) and digital elevation model (DEM) for data processing, and generated the canopy height model (CHM); they obtained a minimum and maximum relative error of tree height of 0.81% and 23.48%, respectively, and estimation accuracy of 90.8% [27]. Lin et al. used LiDAR point cloud to extract information such as the tree height, achieving an accuracy of more than 80% [28]. Mu et al. classified the point clouds from the acquired LiDAR point cloud data to extract ground and vegetation information, achieving a tree height extraction accuracy of over 90% [29]. Liu et al. obtained the point cloud data of trees in sample plots using UAV LiDAR. Then used the improved K-means clustering algorithm and threshold segmentation algorithm based on the relative distance to segment the single-tree point cloud data. The experimental results showed that high accuracy was achieved for individual trees in forest plots segmented using these two algorithms in different evaluation scales; it could distinguish the phenomena of crown overlap, occlusion, and deviation of trees in the forest; and realizes the accurate segmentation of individual trees in the point cloud data of trees in forest plots [30].

The above-mentioned studies focused on single tree height extraction and did not involve extensive tree height extraction

analysis. In this study, a university forest and a power line corridor in Ningxia were selected as the research object, and UAV optical remote sensing and airborne LiDAR were used to extract tree height information, compared the results with the actual height of the trees obtained from the total station. The results showed that the combined use of UAV optical remote sensing and LiDAR enables quick and accurate extraction of tree height information, thus, providing strong support for power-line tree-barrier inspection.

2. Methods

Many technologies are available for power line inspection and tree barrier monitoring, such as UAV remote sensing, airborne LiDAR, and polarization interference synthetic aperture radar [31–33]. These methods differ in terms of the software used and processing, but CHM all use CHM for tree height extraction. Pix4D Mapper 3D modeling software was used in this study to process the images and LiDAR point clouds acquired using a UAV. The technical process is illustrated in Fig. 1. The process can be divided into three main steps.

- (1) The UAV remote sensing images are preliminarily processed to eliminate blank and blurred images. According to the feature points in the image, the 3D model is reconstructed according to the matched feature points and camera position. During 3D model reconstruction, dense point clouds and DSM are obtained. For LiDAR point clouds, denoising generates dense point clouds and DSM.
- (2) For dense point clouds generated from images, the DEM is generated by automatically classifying ground points according to the characteristics of point clouds. For the dense point cloud generated from the point cloud, the Cloth Simulation Filter (CSF) algorithm is used to classify the point cloud, the point cloud is classified into a ground point cloud, and tree point cloud, and the ground point cloud is fitted to generate the DEM.
- (3) CHM is obtained by subtracting the corresponding DSM from the DEM.

The CSF algorithm and focus statistics determine the accuracy of the proposed tree height extraction method.

2.1. Principle of the CSF algorithm

The CSF algorithm can extract the ground point cloud. First, the LiDAR point cloud is flipped upside down to make the ground point cloud up. Next, the effect of gravity on a piece of cloth is simulated. By analyzing the relationship between the cloth node and the corresponding LiDAR point cloud, the final shape of the cloth is determined.

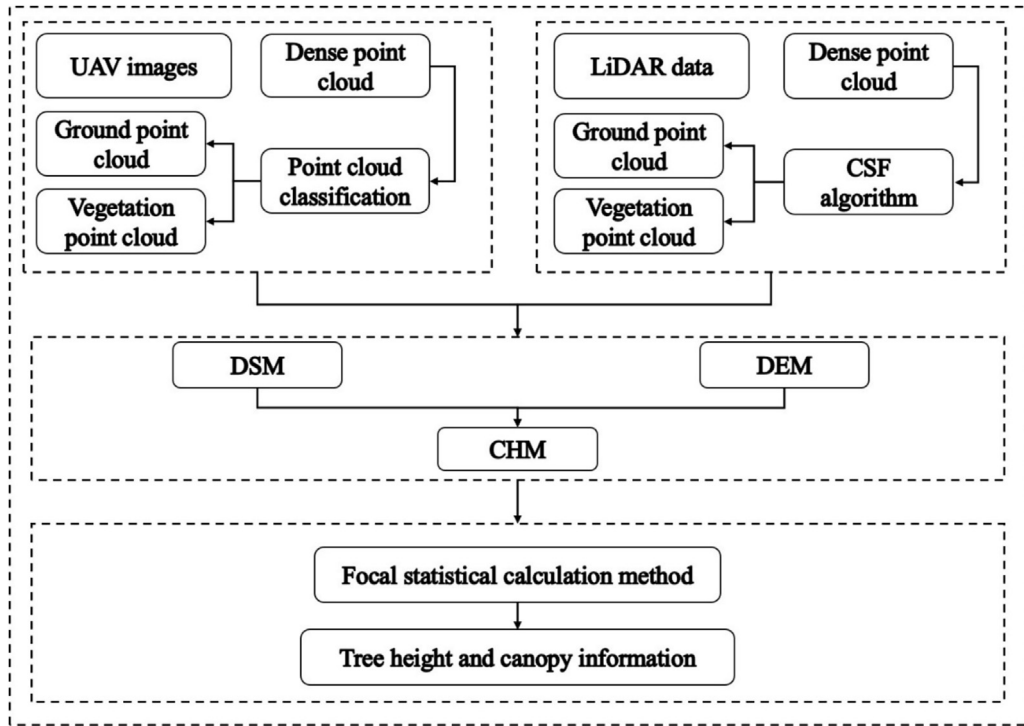
First, an initial Equation is defined:

$$m \frac{\partial X(t)}{\partial t^2} = F_{ext}(X, t) + F_{int}(X, t) \quad (1)$$

where X represents the position of the particles in the cloth at time t , $F_{ext}(X, t)$ represents external driving factors (gravity, collision, etc.), and $F_{int}(X, t)$ represents the internal region factor (the internal connection between particles). The cloth particles are mainly affected by the images of $F_{ext}(X, t)$ and $F_{int}(X, t)$.

The cloth movement process can be described as follows.

- (a) Suppose a virtual cloth is located above the inverted LiDAR point cloud.

**Fig. 1.** Data process flow.

- (b) The influence of gravity on cloth particles is determined. The cloth particles begin to fall, and some cloth particles appear below the ground.
- (c) When the cloth particles fall after the intersection check, it is checked whether the falling cloth particles after the end of the position have reached inside. If yes, then the ground is set as immovable.
- (d) Considering the internal forces of the cloth, the cloth particles are moved to a new position by force generated by the adjacent particles. As can be seen from Eq. (1), the movement of particles is mainly driven by both internal and external factors. Assuming only the external driving force $F_{ext}(X, t)$ and setting the internal driving force $F_{int}(X, t)$ as 0, the following equation can be obtained:

$$X(t + \Delta t) = 2X(t) - X(t - \Delta t) + \frac{G}{m}\Delta t^2 \quad (2)$$

where m represents the weight of the particle (usually set as 1), and Δt is the time step. (2) Can be solved easily as G is a constant. Only a given Δt is required to calculate the new position of the next iteration particle.

To solve the inversion problem of constrained particles in the blank area of the inversion surface, the internal factor $F_{int}(X, t)$ is used. Any two adjacent particles are selected. If both particles are movable, they are moved by the same distance in opposite directions. If one of them is immovable, only the movable one is moved. If both have the same height, they are not moved. The displacement is obtained as follows:

$$\mathbf{d} = \frac{1}{2} b(\mathbf{p}_i - \mathbf{p}_0) \cdot \mathbf{n} \quad (3)$$

where \mathbf{d} is the displacement of the particle. When the particle is movable, $b = 1$; when the particle is immovable, $b = 0$. \mathbf{p}_i is the

adjacent particle of \mathbf{p}_0 , and \mathbf{n} is the unit vector used for normalizing points in the vertical direction $(0, 0, 1)^T$.

The movement process is as follows:

Rigidness (RI) is introduced as a parameter to describe the number of particle movements. When $RI = 1$, movement is performed once by a distance of $1/2$ of the height difference between two particles. When $RI = 2$, movement is performed twice by a distance of $3/4$. When $RI = 3$, the moving distance is $7/8$, and so on. The larger the RI value, the more complex the cloth. The RI value must be set high for flat ground and low for steep slopes and mountainous areas.

2.2. Tree vertex extraction

The gray value of the CHM pixel in CHM denotes the height of the canopy from the ground. The maximum gray value in the center of a single tree crown is identified as the crown vertex, and the gray value of the surrounding area decreases; the tree canopy presents a mountain-like high and a low fluctuation pattern. Major common gray value areas are present between one tree canopy and another, and these areas have an increased pixel brightness. The place with the maximum gray value in CHM is viewed as the tree vertex, and the place with the minimum gray value is regarded as the tree boundary. A place with a small gray value, and the spatial position of an individual tree is obtained. CHM is obtained using DEM and DSM as follows:

$$\text{CHM} = \text{DSM} - \text{DEM}.$$

The grid range of DSM and DEM must be consistent in the calculations.

Tree vertices are extracted using focus statistics and the local maximum method based on the acquired CHM information. First, the appropriate moving window size is set for the selected area. Next, the focus statistics method is used, that is, the neighborhood

calculation of the raster data is performed. When executing the algorithm, each pixel in the grid is accessed to calculate the specified statistical data according to the identified neighborhood. The pixels that are required for calculating the statistical data are called the pixels to be processed, and their values and all the pixel values in the identified neighborhood are included in the calculation of the neighborhood statistical data. The schematic is shown in Fig. 2. A 3×3 rectangular neighborhood is selected. The sum of the pixels to be processed and the surrounding recognition pixels with a value of 5 constitutes the maximum value of the selected field. After all the pixel values in the moving window are determined, a threshold is set; the pixels below the threshold are non-participating and are not included in the tree height calculations. The local maximum algorithm is used to calculate the pixels greater than or equal to the threshold, and the obtained value is the tree vertex of the tree.

3. Experimental analysis

We conducted two case studies on the extraction of tree height information. In case 1, we performed CHM generation by using UAV optical images. The focus statistics of the CHM were used to identify the tree vertices and obtain the height information of trees on campus. In case 2, we received UAV image data and LiDAR point cloud data in a high-voltage transmission line corridor in Yinchuan, Ningxia. We used optical remote sensing and LiDAR data to extract and accurately analyze tree canopy height information under high-voltage transmission-line corridors.

3.1. Case 1

3.1.1. Study area and data source

This study area is located in a university, as shown in Fig. 3. The study area is flat and has a mid-subtropical temperate monsoon climate with abundant rainfall. The tree species in the study area mainly include cypress, osmanthus, and ficus. The crown shape of the cypress is easy to process, and the generated point cloud effect and CHM effect are ideal, which is convenient for identifying the height of trees. The tree density in the region is sparse, which is convenient for single-tree data extraction.

The DJI Phantom 4RTK UAV equipped with an all-in-one camera was used in this experiment. The parameters details are presented in Table 1. To obtain a sufficient number of images for improving the density of the point cloud, we set the flight height as 100 m, heading overlap rate as 84%, and side overlap rate as 72%, and used carrier phase difference technology RTK to measure the control point coordinates. A total of 160 images were obtained during the

UAV flight, with a flight duration of 15 min and a flight area of approximately 0.129 km².

3.1.2. Extraction results obtained using optical remote sensing

First, the aerial triangulation of UAV optical remote sensing images was performed to generate dense point clouds and 3D models of the study area. According to the feature point information of points cloud and 3D models, the digital orthophoto DOM was outputted. Next, the point cloud data in the study area was classified. The point cloud was divided into ground points, vegetation points, power line points, tower points, artificial buildings, and other objects. The ground point cloud and vegetation point cloud were exported to generate the DSM containing only trees and ground, as shown in Fig. 4. The ground point cloud was exported separately and processed to generate the DEM, as shown in Fig. 5. The use of CHM to extract tree height can be divided into the establishment of the CHM and the extracting of tree vertex height. The CHM was obtained using the raster difference between the DSM and DEM. The results are shown in Fig. 6.

The CHM contains information such as canopy size and tree height. According to the characteristics of the canopy in the study area, we used a circular neighborhood for analysis. The neighborhood radius was determined by performing multiple tests based on the crown size and the resolution of the CHM. We used the focus statistical tool to calculate the pixel value in the neighborhood to filter out the maximum point in the neighborhood and determine it as the tree vertex. Next, the incorrect tree vertex was deleted by combining the orthographic image. Finally, the height information of the tree was extracted. The tree vertex extraction results are shown in Fig. 7.

3.1.3. Accuracy analysis of tree height extraction

We extracted the height information of 30 trees and compared the results with the actual tree height data obtained from the total station. Finally, we determined the extraction accuracy by calculating the correlation and absolute error.

As can be seen from Fig. 8(a), the correlation between the tree height extracted using the CHM and the measured height was 0.973. The mean absolute error (MAE) for 30 tree heights was 44.8 cm, the maximum absolute error was 104 cm, and the minimum error was 1.5 cm. These results demonstrate that the UAV images can be used for tree height information extraction.

As can be seen from Fig. 8(b), most of the error values of tree height extracted using UAV images were below 60 cm, and only two errors exceeded 80 cm. The main reason for this phenomenon is that when generating the DEM, some ground points were missed

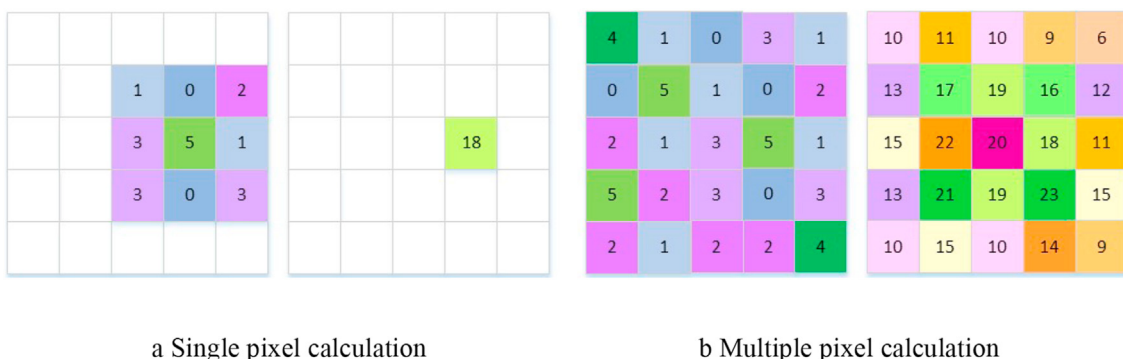


Fig. 2. Principle of focus statistical algorithm.

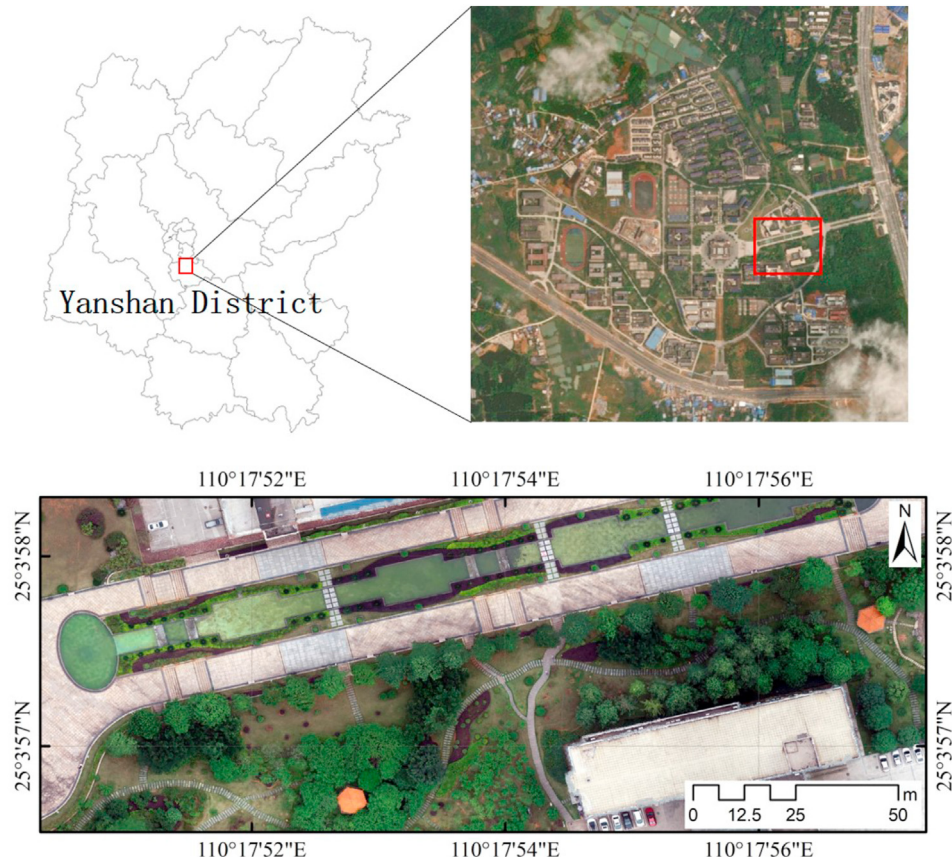


Fig. 3. Study area location.

Table 1
UAV details parameters.

Parameter	Value
Maximum flight speed	58 km/h
PTZ range	−90° to 30°
Satellite positioning module	GPS/BeiDou/Galileo
Image sensor	1 inch CMOS
Camera lens	FOV84f/2.8
Equivalent focal length	35 mm
Effective pixels	20 million
Image maximum resolution	4864×3648

due to the dense canopy of cypress trees, resulting in a poorly generated DEM.

3.2. Case 2

3.2.1. Study area and data source

The study area locates in Xixia District, Yinchuan City, Ningxia Hui Autonomous Region ($38^{\circ}08'$ – $38^{\circ}52'$ N, $105^{\circ}49'$ – $106^{\circ}18'$ E), as shown in Fig. 9, in the western end of the monsoon region of China and has a temperate continental arid and semi-arid climate with four distinct seasons and a large temperature difference between day and night. This region witnesses low annual rainfall (150–600 mm). The trees under the power-line corridor are mainly willows and poplars. The planting interval of willows is large, which is conducive to extracting individual tree height.

The study area is located next to a field, with many power lines around it. There are no artificial buildings in the study area except

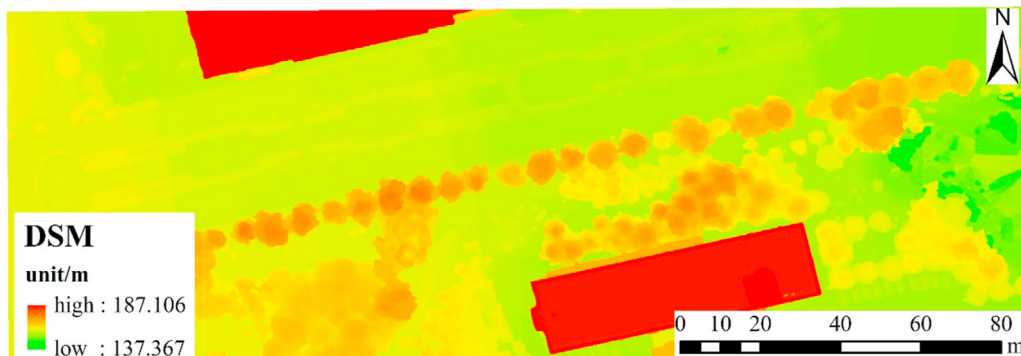
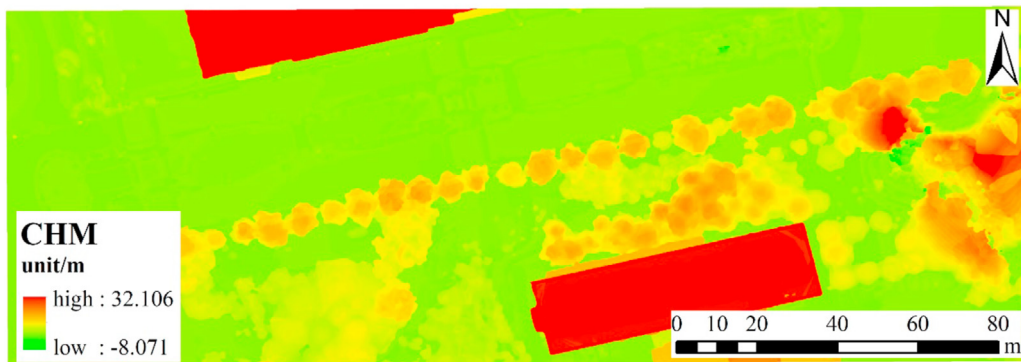
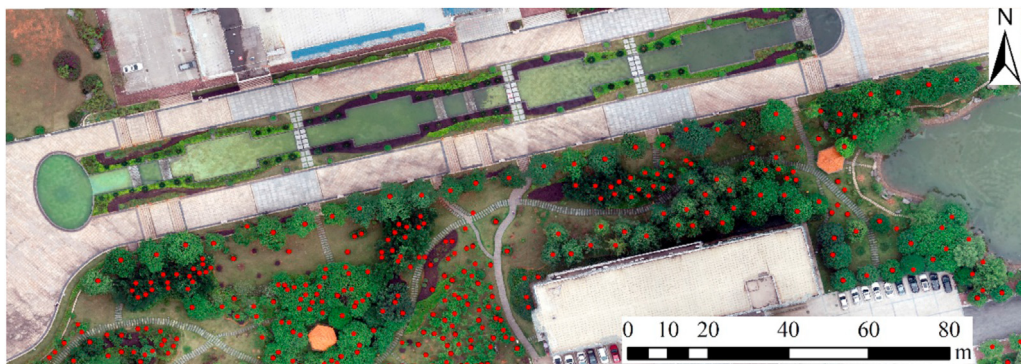
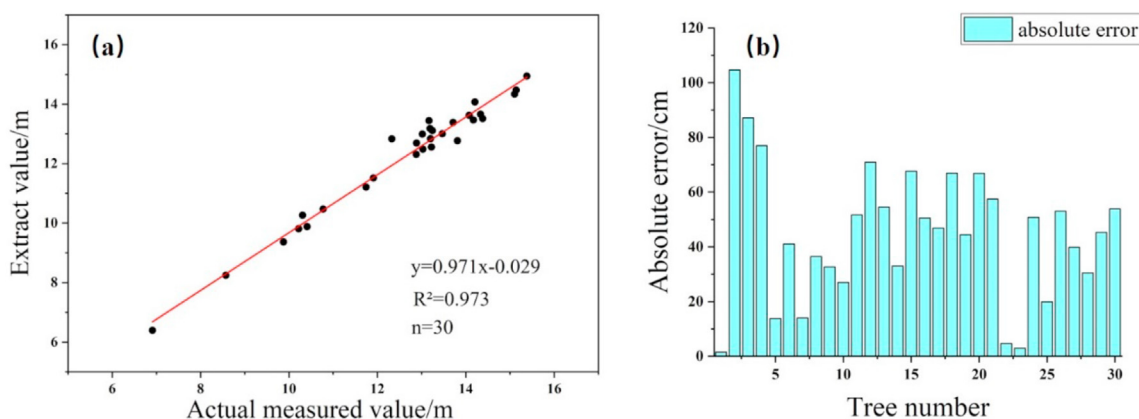


Fig. 4. Digital surface model.

**Fig. 5.** Digital elevation model.**Fig. 6.** Canopy height model.**Fig. 7.** Identification of tree vertices.**Fig. 8.** Linear analysis (a), and absolute error (b) of the tree height extraction.

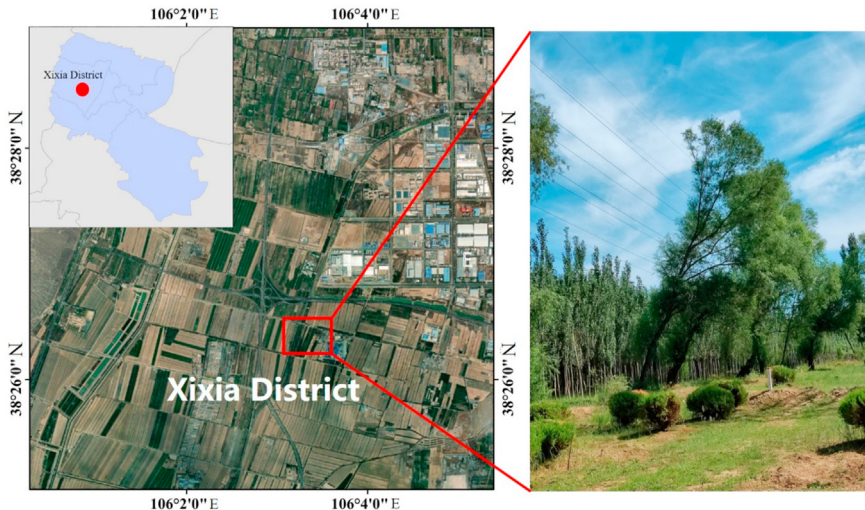


Fig. 9. Study area location.

power lines. On the data collection day, the weather was clear and windless. Two sets of data were collected. First, the optical remote sensing image data were obtained using the DJI Phantom 4RTK UAV at the height of 100 m (Fig. 10); the heading overlap rate was 80%, and the side overlap rate was 75%. The second data group was airborne LiDAR data, and the UAV used was DJI M300 RTK. The UAV is equipped with a LiDAR sensor, which scans the ground horizontally to obtain the distance parameters between the ground point and the sensor. The aircraft relies on GPS navigation to achieve longitudinal flight, enabling the LiDAR sensor to get LiDAR data over the entire surface plane. The UAV and LiDAR sensor parameters are presented in Table 2.

3.2.2. Tree height extraction based on airborne LiDAR

3.2.2.1. Tree height extraction from airborne LiDAR

The original airborne LiDAR data were processed to obtain the point cloud data. First, the statistical filtering method was used to

Table 2
M300 UAV parameters.

Parameter	Value
Maximum flight speed	83 km/h
Equipped with sensors	DJI L1
Satellite positioning module	GPS/BeiDou/Galileo/GLONASS
Image sensor	1 inch CMOS
Turn angle	depression angle: -120° to 30° straight angle: 320°
Point cloud data rate	Single echo: 240,000 points/s Multiple echo: 480,000 points/s
Maximum number of echoes	3
Image maximum resolution	4864×3648

denoise the point cloud to improve its quality of the point cloud. The DSM was generated based on the point cloud, as shown in Fig. 11. CSF calculation was performed on the point cloud to separate the ground points and non-ground points from the point cloud.

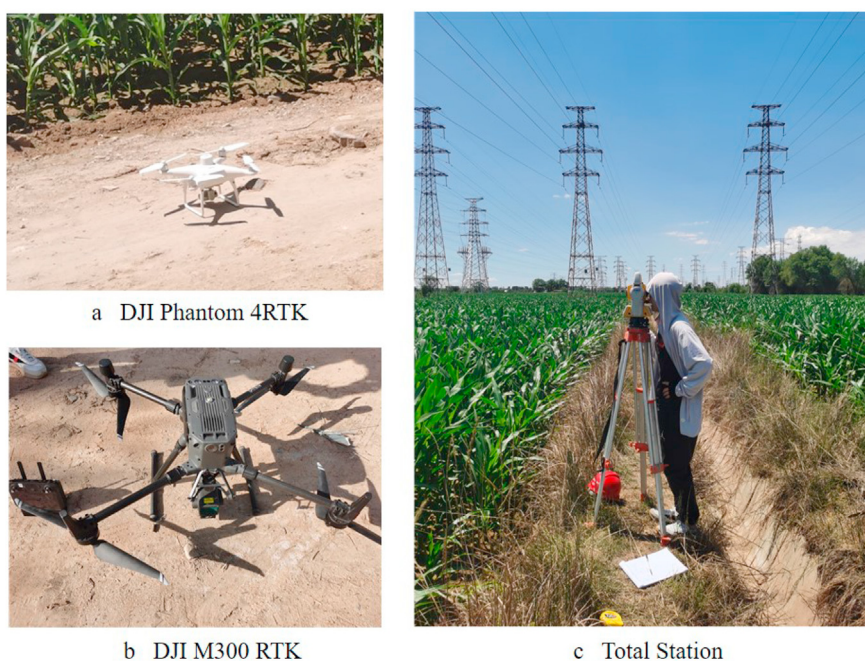


Fig. 10. Experimental instrument.

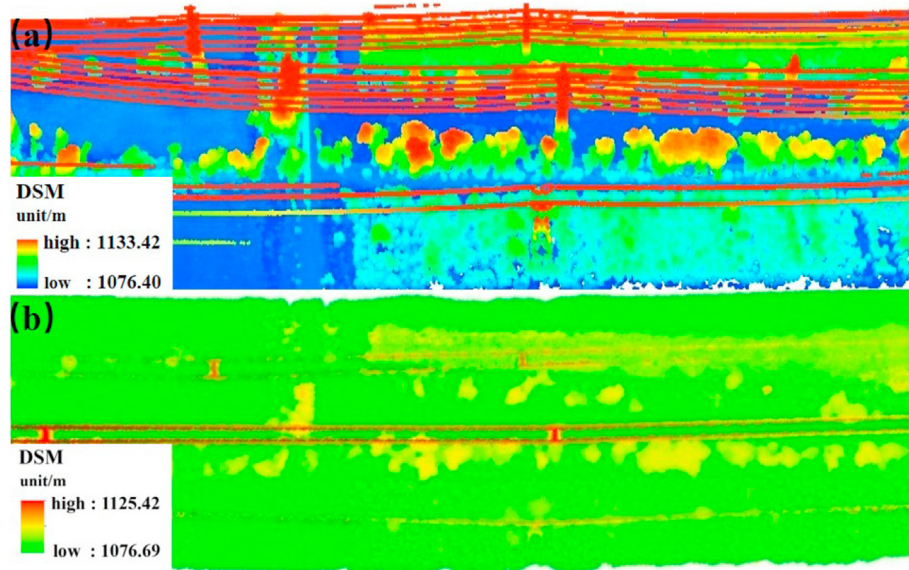


Fig. 11. Point cloud data and generated DSM.

The DEM was generated by refitting the ground point clouds, as shown in Fig. 12, and the point cloud was normalized, and the terrain image was removed. The parameters such as tree height, crown area, crown volume, and single tree position were obtained by segmenting the point cloud for a single tree. Then, the parameters were used to obtain the tree height information based on the LiDAR point cloud information. Furthermore, the CHM was obtained from the raster difference between the DSM and DEM, as shown in Fig. 13. Finally, the individual tree information extracted using the point cloud data was compared with the individual tree information extracted using the CHM.

3.2.2.2. Extraction results and accuracy analysis

30 trees in the study area were employed as the research object. The tree height based on LiDAR point cloud information extraction and the tree height extracted by CHM based on LiDAR point cloud generation were obtained respectively. The extraction results are shown in Fig. 14. The extracted tree heights range from 10 to 15 m.

Due to the limitations posed by the complex terrain, we conducted field measurements on eight trees, as shown in Table 3. The tree height data extracted using the LiDAR point cloud and CHM and the measured tree height were compared and analyzed. The tree height extracted using the CHM exhibited a large error because the extraction was performed using the canopy model. Because the ficus tree canopy was scattered and conical, the tree top was smoothed during the generation of DSM, resulting in a decreased height. In contrast, because the roots of some ficus trees were relatively thick, they were mistaken for the ground, increasing the elevation of the base of the tree, eventually leading to a deviation between the height obtained using the generated canopy model and the measured tree height. Next, the linear regression equations were established for these eight trees.

The linear relationship between the tree height extracted using the airborne LiDAR point cloud data and the measured tree height is depicted in Fig. 15. The linear regression equation was $y = 0.953x + 0.085$, the regression coefficient was 0.953, and the determination coefficient R^2 was 0.947. The tree height obtained using airborne LiDAR exhibited an excellent linear relationship with the actual measured tree height.

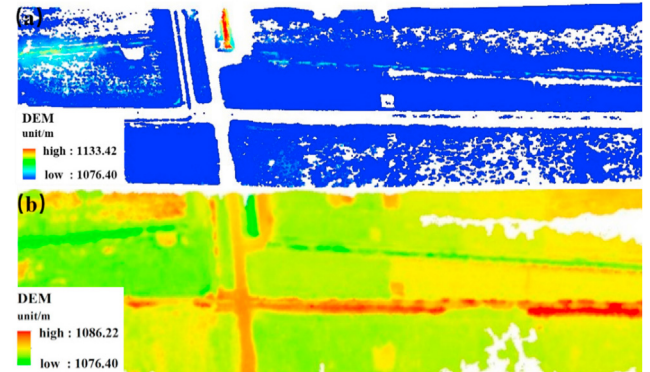


Fig. 12. Ground point cloud and generated DEM.

The linear relationship between the measured tree height and the tree height obtained using the CHM is shown in Fig. 16. The linear regression equation was $y = 0.946x + 0.059$, the regression coefficient was 0.946, and the determination coefficient R^2 was 0.931. The comparison of the correlation between the two revealed that the tree height extracted using the airborne LiDAR point cloud information and the CHM generated using the point cloud can well extract the tree height information.

3.2.3. Integrating UAV optical remote sensing imagery with LiDAR for tree height information extraction

In the process of aerial photography of UAV images in the study area, due to the influence of wind factors in the area at that time, safety issues were considered, the area taken by the DJI Phantom 4RTK we used does not contain trees measured in the field, but most of the point cloud areas flying by the DJI M300 RTK overlap. Therefore, we extracted the overlapping area separately and generated the DSM, DEM, and CHM based on the UAV images and LiDAR point clouds, as shown in Fig. 17. The model features generated using the two data sources were identical, and the identified trees were visible. The CHM generated using the two data sources extracted the tree height information better and yielded a higher accuracy. By analyzing the tree barriers in transmission-line

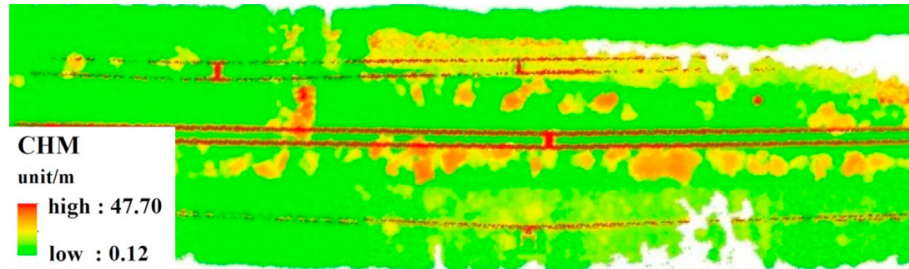


Fig. 13. The generated CHM.

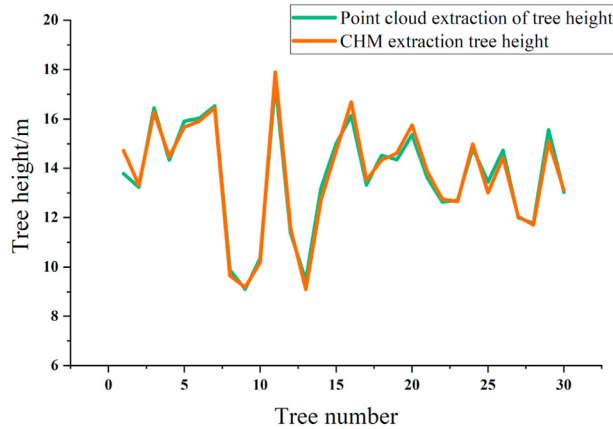


Fig. 14. Comparison of extraction results shows.

corridors using optical remote sensing and LiDAR, power line inspection can be performed in an advanced, scientific manner.

4. Analysis

4.1. Accuracy analysis using different methods

The height of the trees on the university campus was extracted based on UAV images. Then the height of the tree barriers under the power-line corridor was extracted using airborne LiDAR. We studied the UAV and airborne LiDAR accuracy of different methods, as shown in Table 4.

Different methods were used to extract the tree height information. The tree height information was better extracted using point cloud and CHM. The average absolute error of tree height extracted using UAV images, point cloud, and CHM was 44.8, 11.1, and 30.4, respectively. The tree height extracted using UAV remote

Table 3

Tree height and error results were obtained using three methods. Absolute error 1 represents the difference between the tree height extracted using the point cloud information and the measured tree height. Absolute error 2 represents the difference between the tree height extracted using the CHM and the measured tree height. Relative error 1 represents the ratio of the absolute error to the true value of the tree height extracted using the point cloud information. Relative error 2 represents the ratio of the absolute error to the true value of the tree height extracted using the CHM.

Number	Point cloud information extraction tree height (m)	CHM extract tree height (m)	Measured tree height (m)	Absolute error 1(m)	Absolute error 2(m)	Relative error 1 (%)	Relative error 2 (%)
1	13.767	14.721	13.788	-0.021	0.933	-0.155	6.764
2	14.230	13.310	13.627	-0.397	-0.317	-2.911	-2.324
3	16.449	16.260	16.379	0.070	-0.119	0.425	-0.729
4	14.326	14.480	14.265	0.061	0.215	0.428	1.507
5	15.910	15.672	15.858	0.052	-0.186	0.327	-1.174
6	16.033	15.915	16.113	-0.080	-0.198	-0.497	-1.230
7	16.528	16.443	16.706	-0.178	-0.263	-1.063	-1.572
8	9.883	9.650	9.853	0.030	-0.203	0.307	-2.057

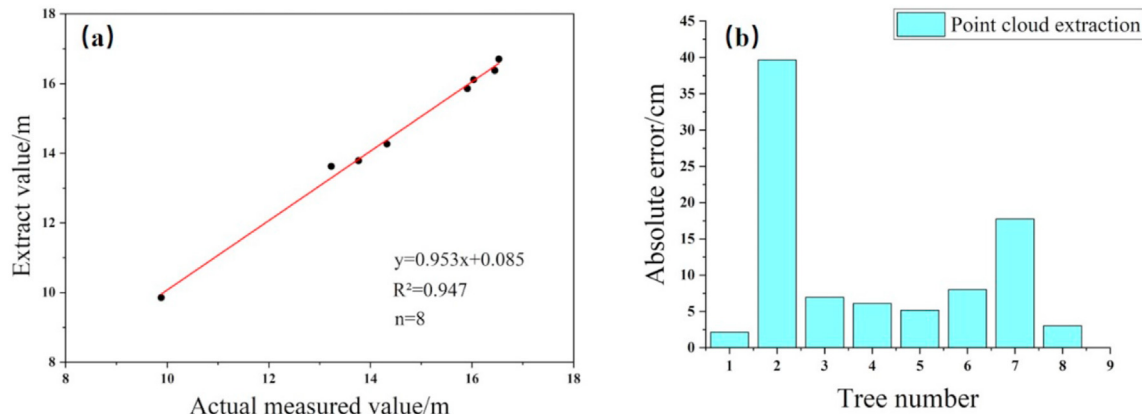


Fig. 15. High precision comparison based on point cloud extraction tree.

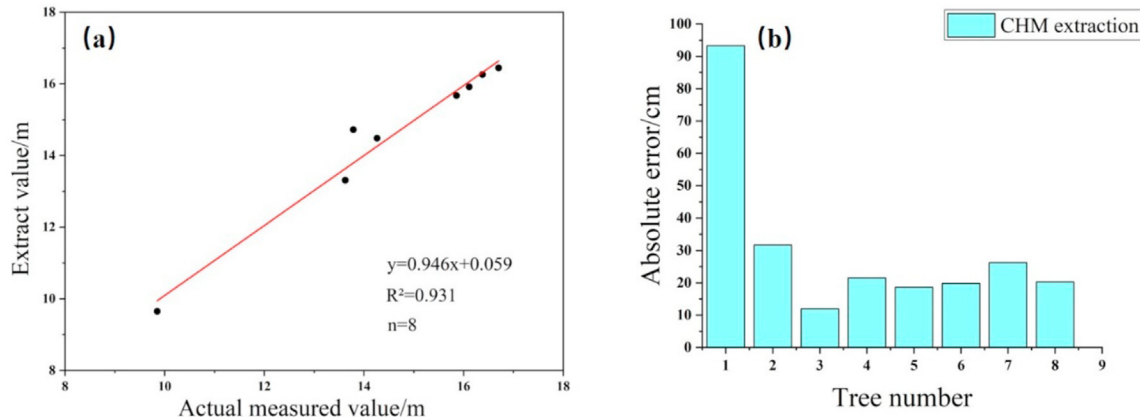


Fig. 16. High precision comparison based on CHM extraction tree.

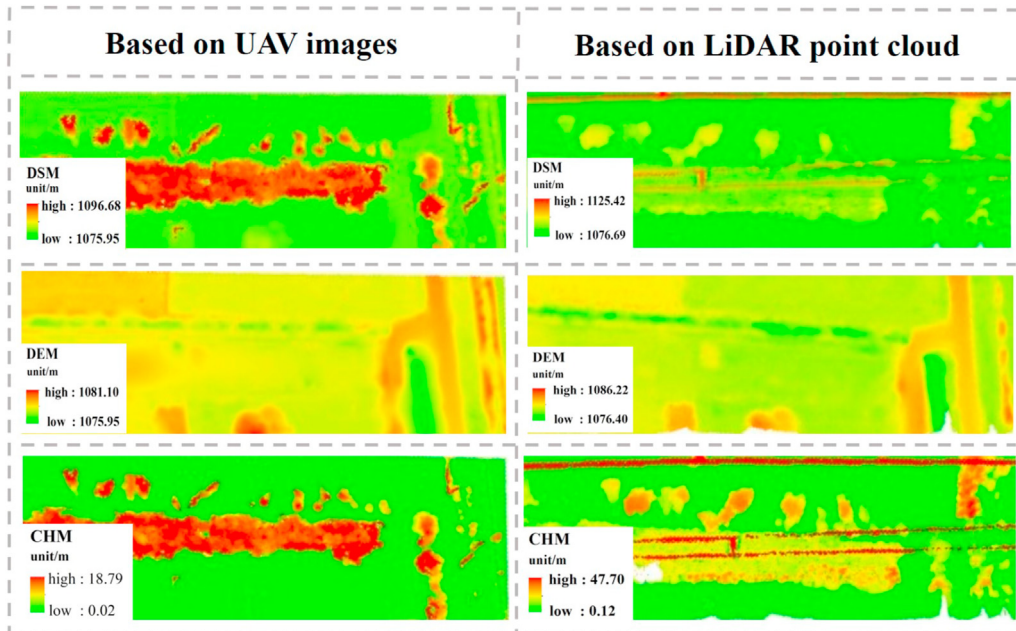


Fig. 17. Model comparison of different data sources.

sensing was based on the 3D reconstruction of UAV images to obtain the point cloud. When the UAV encountered a high vegetation density, it failed to obtain the ground points. Thus, the DEM generated based on UAV remote sensing was biased, leading to inaccurate tree height extraction results. In contrast, the airborne LiDAR, owing to its strong penetration ability, penetrated leaves to obtain the ground points. Thus, the generated DEM was more accurate, and the extracted tree height data was highly accurate.

4.2. Accuracy analysis for different tree species

In addition to the influence of extraction methods on the accuracy of tree height, the extraction accuracy varies for different tree species. The point clouds and actual scenario for different tree species are shown in Fig. 18. The extraction effect for cypress trees was better than that for willow trees. As shown in Fig. 18, obvious differences exist between the two trees. The crown shape of the cypress is uniform, thus, resulting in better point cloud rendering. In contrast, the crown shape of willow is relatively non-uniform with irregular dispersion; thus, the point cloud rendering effect is worse than that for cypress. Moreover, when

Table 4
Accuracy of different methods.

	UAV extracts tree height	Airborne LiDAR extraction of tree height	
		Point cloud extraction	CHM extraction
R^2	0.973	0.947	0.931
MAE (cm)	44.8	11.1	30.4

extracting the cypress tree vertex, the crown is easier to split out, aiding in determining the height of the tree. In contrast, willow trees have a flatter canopy area, which leads to two or more tree vertex when extracting the tree height, resulting in inaccurate tree height extraction.

4.3. Tree height extraction error analysis

Tree height extraction on the campus was performed using the CHM generated using UAV images. The error was mainly due to the process of refitting the ground points to generate DEM after point cloud classification. The field survey revealed that the terrain in the study area is uneven. Thus, when the DEM was regenerated, the

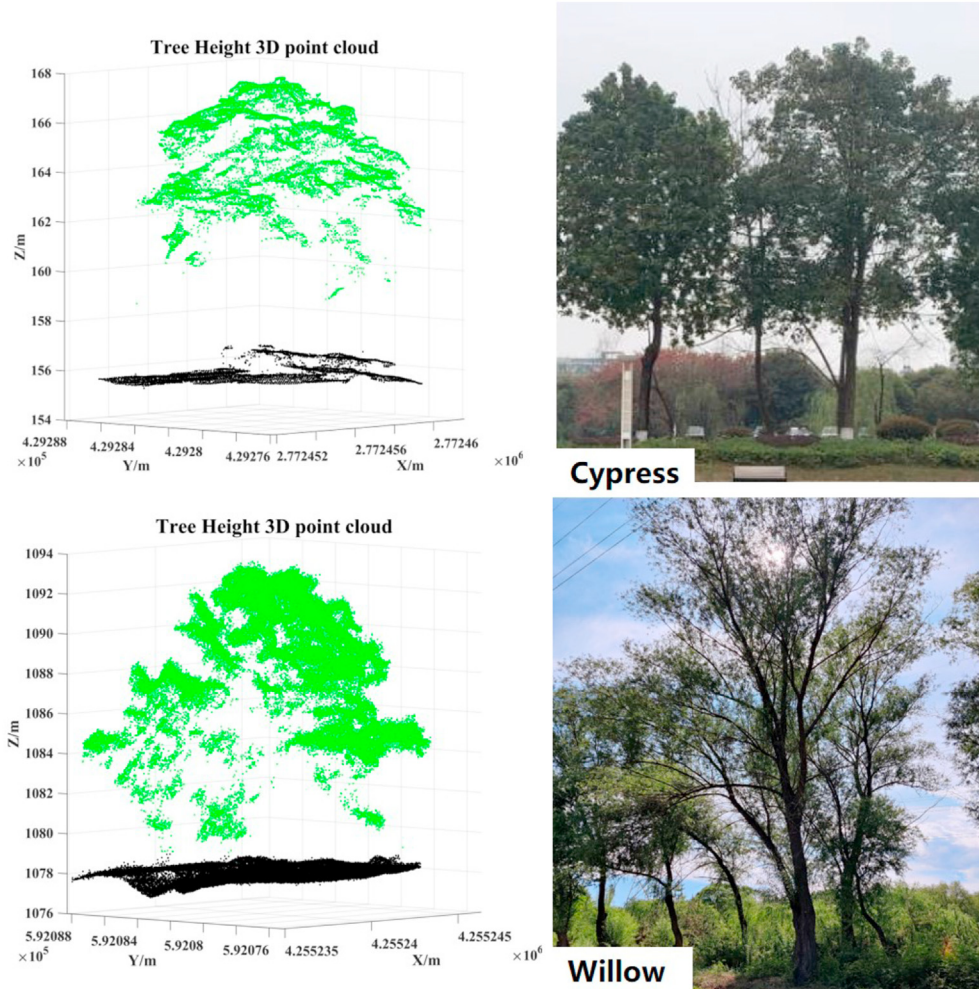


Fig. 18. Point cloud extraction results of different tree species.

position of the original tree root was fitted to other planes, resulting in a decrease in the height of the extracted trees.

In Ningxia, willow trees were selected as the research object. The height of the trees in the power-line corridor was extracted using optical remote sensing and airborne LiDAR. The experimental results revealed that the extraction of the tree barrier height by using UAV and airborne LiDAR is highly feasible. The height information of 30 trees was extracted, and the height information of eight trees was measured. Statistical analysis revealed that when the height of trees was 11–13 m, the accuracy of tree height obtained using UAV images and that extracted by airborne LiDAR decreased. Field investigation revealed that when the height of trees was 11–13 m, the vegetation coverage rate was higher than that at other heights, which is not conducive to the penetration of light and LiDAR, resulting in a slight loss of ground point information acquisition.

Tree height extraction in Ningxia was more complex than on campus. The resolution of the generated CHM, the size of the smoothing window, and the size of the moving window affected the extraction of the tree vertex in Ningxia. The number of tree vertices extracted was inversely proportional to the smoothing window size and the moving window size. When the smoothing window was the same size as the moving window, the number of extracted tree vertices was proportional to the resolution of the CHM. Because the experimental site was located at a high altitude, the UAV was greatly affected by the external environment during flight, involving the generation of the CHM. When the tree vertices

were extracted for CHM generation, the number of tree vertices extracted was more than one because, for denser trees, the branches of the tree were at the same height as the top point of the tree, and the highest point of the branch was mistaken as the top point of the tree. In addition, the tree crowns were uneven, and the trees with larger crowns obscured the tree vertex of smaller trees, resulting in the omission of the tree vertex. For the misjudgment and omission of the tree vertex, in the focus statistics, according to the shape and size of the crown width of the tree species in the study area and the characteristics of the trees in the horizontal and vertical directions, multiple experiments were performed to select the appropriate shape and value for domain analysis to improve the extraction accuracy of the tree vertex.

5. Conclusions

In this study, we used UAV optical remote sensing and LiDAR to measure the height of trees in a high-voltage transmission-line corridor in a university and Ningxia and performed an accuracy analysis. The following conclusions can be drawn:

In the case of tree height extraction by using UAV optical images, 22 out of the 30 trees exhibited a relative error of less than 5%, with the lowest relative error being 0.11%. The coefficient of determination R^2 between the optical image tree height extraction results and the measured tree height was 0.97, demonstrating that UAV image data can be used to measure tree height with high accuracy.

In on-field tree-barrier monitoring of high-voltage transmission lines in Ningxia, the tree height extracted using airborne LiDAR point clouds and CHM were compared and analyzed with the measured tree heights, and the determination coefficients R^2 were obtained as 0.947 and 0.931, respectively. The maximum and minimum relative errors of the tree heights obtained using the point cloud were 2.91% and 0.15%, respectively, and the maximum and minimum relative errors of the tree heights obtained using CHM were 6.76% and 0.7%, respectively, with an extraction accuracy of over 95%. The results of both experiments validated the feasibility of optical remote sensing with airborne LiDAR for extracting the height of tree barriers in power-line corridors. Based on the advantages of optical remote sensing and LiDAR, the proposed integrated optical remote sensing and LiDAR-based tree height recognition method can extract tree obstruction information more quickly and effectively. They can provide more effective data support for power-line inspection.

During the experiments, several major sources of error affected the accuracy of tree height extraction:

- When generating the DSM, the highest points of the trees were often processed together by model smoothing.
- High-density vegetation in some areas led to the absence of ground point clouds when reconstructing the 3D point cloud model, making the generated DEM less accurate.
- The terrain around the trees was undulating, and the relevant point clouds were not accurately categorized during point cloud classification, decreasing the resolution of the generated CHM.

In future research, we can try new extraction methods or develop new algorithms to improve the resolution of CHM and the accuracy of tree monitoring. Currently, there are problems in the monitoring of tree barriers by using UAVs. For the extraction of tree height information, ground images are required to generate ground elevation; however, the UAVs cannot capture ground information due to canopy obstruction. Therefore, how to better use UAVs for tree-barrier detection and improve their measurement accuracy still needs further research.

Declaration of competing interest

The authors declare that there is no conflicts of interest.

Acknowledgments

The authors declare that there are no conflicts of interest. This research was funded by Key R&D project of Ningxia Hui Autonomous Region (2021BDE931027); Science and technology project of State Grid Ningxia Electric Power Co. Ltd. (229DK2004P).

References

- M. Shahbaz, H.H. Lean, Does financial development increase energy consumption? The role of industrialization and urbanization in Tunisia, *Energy Pol.* 40 (2012) 473–479.
- R. Madlener, Y. Sunak, Impacts of urbanization on urban structures and energy demand: what can we learn for urban energy planning and urbanization management, *Sustain. Cities Soc.* 1 (2011) 45–53.
- L. Matikainen, M. Lehtomäki, E. Ahokas, et al., Remote sensing methods for power line corridor surveys, *ISPRS J. Photogramm. Remote Sens.* 119 (2016) 10–31.
- J. Ahmad, A.S. Malik, L. Xia, et al., Vegetation encroachment monitoring for transmission lines right-of-ways: a survey, *Electr. Power Syst. Res.* 95 (2013) 339–352.
- H. Guan, X. Sun, Y. Su, et al., UAV-lidar aids automatic intelligent powerline inspection, *Int. J. Electr. Power Energy Syst.* 130 (2021), 106987.
- H. Zhao, S. Huang, Study on electric field variation characteristics and critical breakdown distance of 110kV transmission line near trees, *Comput. Digit. Eng.* 48 (2020) 2057–2063.
- A.B. Bala, X. Zhang, X. Shen, et al., Power transmission line inspection robots: a review, trends and challenges for future research, *Electr. Power Energy Syst.* 118 (2020), 105862.
- W. Bo, D. Wang, Y. Zhao, et al., Rapid positioning method of power line inspection unmanned aerial vehicle assisted by BeiDou ground-based augmentation station, *Energy Rep.* 7 (2021) 1139–1148.
- H.H. Alhelou, M.E. Hamedani-Golshan, T.C. Njenda, et al., A survey on power system blackout and cascading events: research motivations and challenges, *Energies* 12 (2019) 682.
- A.D. Syphard, J.E. Keeley, Location, timing and extent of wildfire vary by cause of ignition, *Int. J. Wildland Fire* 24 (2015) 37–47.
- Y. Chen, J. Lin, X. Liao, Early detection of tree encroachment in high voltage powerline corridor using growth model and UAV-borne LiDAR, *Int. J. Appl. Earth Obs. Geoinf.* 108 (2022) (2022), 102740.
- H. Zeng, Q. Yang, X. Ma, et al., Simulation test on the characteristics of pre-discharge for tree fault under transmission line, *Electr. Eng.* 21 (2020) 93–97.
- H. Xie, Z. Wen, S. Zhong, et al., Measure method research of tree height and tree crown by non-prism total station, *J. Centr. South Univ. Forest. Technol.* 31 (2011) 53–58.
- X. Huang, Z. Feng, M. Xie, et al., Developing and accuracy analysis of portable device for automatically measuring diameter at breast height and tree height, *Trans. Chin. Soc. Agric. Eng.* 31 (2015) 92–99.
- D. Yu, Z. Feng, Z. Cao, et al., Error analysis of measuring diameter at breast height and tree height and volume of standing tree by total station, *Trans. Chin. Soc. Agric. Eng.* 32 (2016) 160–167.
- D. Zhao, Individual tree parameters extraction based on LiDAR and hyperspectrum data, *Chin. Acad. Forest.* (2012).
- Z. Sun, F. Wu, X. Gao, et al., Estimation of forest canopy height based on large-footprint airborne LiDAR data, *Forest Resour. Manag.* (2020) 111–117.
- X. Deng, G. Tang, Q. Wang, A novel fast classification filtering algorithm for LiDAR point clouds based on small grid density clustering, *Geod. Geodyn.* 13 (2022) 38–49.
- S.R. Cloude, K.P. Papathanassiou, Three-stage inversion process for polarimetric SAR interferometry, *IEE Proc. - Radar, Sonar Navig.* 150 (2003) 125–134.
- Q. Xie, J. Zhu, C. Wang, et al., A modified dual-baseline PolInSAR method for forest height estimation, *Remote Sens.* 9 (2017) 819.
- Y. Wu, J. Zhu, H. Fu, et al., Three-stage of polarimetric interferometric coherence optimization vegetation height inversion process, *Bull. Surv. Mapp.* (2016) 32–35+76.
- B. Xiong, X. Li, Offset measurements along active faults based on the structure from motion method—a case study of Gebiling in the Xorkoli section of the Altyn Tagh Fault, *Geod. Geodyn.* 11 (2020) 358–366.
- K. Strzabal, P. Ćwiakala, W. Gruszczynski, et al., Determining changes in building tilts based on UAV photogrammetry, *Measurement* 202 (2022), 111772.
- J.B. Sankey, T.T. Sankey, J. Li, et al., Quantifying plant-soil-nutrient dynamics in rangelands: fusion of UAV hyperspectral-LiDAR, UAV multispectral-photogrammetry, and ground-based LiDAR-digital photography in a shrub-encroached desert grassland, *Remote Sens. Environ.* 253 (2021), 112223.
- O.G. Ajayi, M. Palmer, A.A. Salubi, Modelling farmland topography for suitable site selection of dam construction using unmanned aerial vehicle (UAV) photogrammetry, *Remote Sens. Appl.: Soc. Environ.* 11 (2018) 220–230.
- Y. Zhao, L. Zhou, Y. Pan, et al., Accuracy verification of danger tree monitoring for general consumer UAV, *Bull. Surv. Mapp.* (2021) 159–164.
- Q. Xie, K. Yu, Y. Deng, et al., Height measurement of Cunninghamia lanceolata plantations based on UAV remote sensing, *J. Zhejiang A & F Univ.* 36 (2019) 335–342.
- Y. Lin, H. Ji, Q. Ye, Research on method of extracting single tree characteristics from lidar point, *Comput. Meas. Control* 25 (2017) 142–147.
- X. Mu, Q. Zhang, Q. Liu, et al., Inversion of forest height and canopy closure using airborne LiDAR data, *J. Northeast For. Univ.* 43 (2015) 84–89.
- H. Liu, W. Fan, Y. Xu, et al., Research on single tree segmentation based on UAV LiDAR point cloud data, *J. Centr. South Univ. Forest. Technol.* 42 (2022) 45–53.
- O.B. Schofield, N. Iversen, E. Ebeid, Autonomous power line detection and tracking system using UAVs, *Microprocess. Microsyst.* 94 (2022), 104609.
- H. Guan, X. Sun, Y. Su, T. Hu, et al., UAV-lidar aids automatic intelligent powerline inspection, *Int. J. Electr. Power Energy Syst.* 130 (2021), 106987.
- T. Fatoyinbo, J. Armston, M. Simard, et al., The NASA AfriSAR campaign: airborne SAR and lidar measurements of tropical forest structure and biomass in support of current and future space missions, *Remote Sens. Environ.* 264 (2021), 112533.



Jinpeng Hao, was born in Heilongjiang, China in 1985. He graduated from North China Electric Power University in 2008 and is now a senior Electric Power Research Institute engineer at Guowang Ningxia Electric Power Co., Ltd. Senior engineer, engaged in power grid equipment testing and technical supervision and other work.